Applied Catalysis B: Environmental 245 (2019) 496–501

Contents lists available at ScienceDirect

Applied Catalysis B: Environmental

journal homepage: www.elsevier.com/locate/apcatb

Photosensitizing single-site metal – organic framework enabling visible-light-driven CO_2 reduction for syngas production

Meng Liu[a], Yan-Fei Mu[a], Shuang Yao[b,*], Song Guo[a], Xiang-Wei Guo[a], Zhi-Ming Zhang[a,*], Tong-Bu Lu[a]

[a] Institute for New Energy Materials & Low Carbon Technologies, School of Material Science & Engineering, Tianjin University of Technology, Tianjin, 300384, People's Republic of China

[b] Tianjin Key Laboratory of Organic Solar Cells and Photochemical Conversion, School of Chemistry and Chemical Engineering, Tianjin University of Technology, Tianjin, 300384, People's Republic of China

ARTICLE INFO

Keywords:
Metal-organic framework
CO_2reduction
Syngas
Photosensitizer
Photocatalyst

ABSTRACT

Photocatalytic CO_2 reduction into syngas (CO and H_2) is one of sustainable strategies for recycling CO_2 into value-added products. Herein, a simple and effective two-step self-assembly process was developed to functionalize phosphorescent metal-organic framework (MOF) with single site catalyst. The resulting $(Co/Ru)_n$-UiO-67(bpydc) supplied molecular platform to enable fast multielectron injection from photosensitizers (PSs) to Co-catalyst, leading to the first MOF-based composite photocatalyst for efficient syngas production with a yield of 13,600 $\mu mol \cdot g^{-1}$ (H_2 : CO = 2 : 1) in 16 h, 29.2-fold higher than that of its homogeneous counterpart. The H_2/CO ratios can be well controlled by carefully adjusting the molar ratio of PS/catalyst in the MOF platform and the water content in the photocatalytic system. This work provides a prospective strategy for recycling CO_2 into H_2-rich syngas by merging PSs and single-site catalysts into a MOF platform.

1. Introduction

Metal-organic frameworks (MOFs) are an unique class of porous molecular solid material constructed from tunable metal nodes and organic linkers. Owing to the high surface areas and well-ordered porous structure, the emerging class of functional porous hybrid materials have been applied in widespread applications, such as gas adsorption and separation, drug delivery, luminescent sensors, and catalysis [1–11]. Recently, MOFs have been widely used as molecular platform to study light-absorption and single-site catalysis [12,13]. In this field, great progress has also been achieved in assembly of antenna molecules or catalysts into MOFs to afford photocatalytic systems for water splitting, CO_2 reduction and organic photoreactions [14–18]. However, these photocatalytic systems are usually constructed from single active component that served as efficient catalysts or the role of photosensitization. In this process, simultaneous incorporation of photosensitizers (PSs) and catalysts into MOFs have proven to be an effective strategy for the construction of composite molecular catalytic system with enhanced photocatalytic performance [19]. For example, Lin et al introduce Pt NPs, Wells-Dowson POM and transition-metal substituted Sandwich-type POMs into photosensitizing MOFs to dramatically enhance their photocatlytic performance for hydrogen evolution reaction (HER) [20–22]. Parkand et al. functionalized bipyridine-embedded UiO-67 with a molecular Pt(II) or Co catalyst and PS to afford an efficient photocatalytic system for HER [23–25]. These results all demonstrate that incorporation of PSs and catalysts into MOFs represents an effective strategy for enhancing their photocatalytic HER performance, however, their applications in photocatalytic CO_2 reduction are rarely explored.

CO_2 reduction reaction (CO_2RR) represents a promising technology for energy storage and carbon recycling, providing a way to mitigate the environmental crisis caused by greenhouse CO_2 emissions from fossil fuel utilization [26]. To date, great effort has been paid to promote the transformation of CO_2 toward a sustainable energy circle into valuable chemicals and fuels [27]. Among all the possible technological routes, visible-light-driven two-electron reduction of CO_2 to CO is a kinetically favorable choice because of its lower reaction barrier compared to that of one-electron and other multi-electron reactions [28,29]. Besides, CO as the main component of syngas (a mixture of H_2 and CO) is widely used in the synthesis of valuable hydrocarbons in various industries. Furthermore, syngas is a versatile fuel precursor for producing chemical and synthetic liquid fuels, and tunable H_2/CO ratios in syngas mixtures are the key factors to meet the requirements of different industrial productions [30,31]. Currently, syngas is

* Corresponding authors.
E-mail addresses: shuangyao@email.tjut.edu.cn (S. Yao), zmzhang@email.tjut.edu.cn (Z.-M. Zhang).

https://doi.org/10.1016/j.apcatb.2019.01.014
Received 1 November 2018; Received in revised form 20 December 2018; Accepted 6 January 2019
Available online 07 January 2019
0926-3373/

predominantly produced by the gasification of coal or the steam reforming of natural gas, which largely consumes non-renewable fossil sources and requires harsh synthetic conditions. As well known, photochemical reduction represents an ideal way for CO_2 reduction under mild conditions, which always accompanies with hydrogen evolution in the aqueous solution. Thus, photocatlytic CO_2RR in aqueous solution will open an avenue for continual production of syngas, and provide a promising strategy to respond the energy and environmental crisis [32–35]. Moreover, adjusting the ratio of H_2/CO in syngas mixtures is critical, for example, 2:1 H_2/CO is critical for methanol and Fischer-Tropsch synthesis [36]. Up to date, it is still great challenge to design and synthesize efficient catalysts for reducing CO_2 into syngas with controllable composition as the chemical inertness and the complex conversion process of CO_2.

Recently, numerous efforts have been made and dedicated to design and construction of high-efficiency photocatalysts for CO_2 reduction. In this filed, dimeric Co-complexes, Re and Mn-based molecules with well-defined structure, and single atom Co catalysts have been developed as catalysts for CO_2 reduction to provide definite structure-activity relationship for further exploring high-efficiency catalysts [2,10,28,37–39]. Considering the success of MOFs in artificial photosynthesis, great progress has been made for CO_2 reduction by using MOFs as carrier to support active sites or PS, such as, Zhang et al. used Co-based MOF for photocatalytic reduction of CO_2 to CO [28]. Kong et al constructed an Eu-based MOF with Ru(phen)$_3$-derived ligands to catalyze visible-light-driven CO_2 reduction into formate [40]. Jiang et al. reported a porphyrin involved MOF that can selectively capture and further reduce CO_2 under visible-light irradiation [41]. Wang et al reported hybrid $Cd_{0.2}Zn_{0.8}S$@UiO-66-NH_2 nanocomposites with excellent stability during photocatalytic H_2 evolution and CO_2 reduction [42]. Incorporation of PS and single site catalysts into a MOF represents a very interesting field for photocatalytic CO_2 reduction, however their application related to the syngas production is rarely explored.

Herein, a simple and effective two-step self-assembly process was developed to functionalize phosphorescent MOF with single site catalyst. The resulting (Co/Ru)$_{2.4}$-UiO-67(bpydc) molecular platform enables fast multielectron injection from antenna molecules to cobalt catalysts, leading to the first MOF-based photocatalyst for efficient syngas production with a yield of 13,600 μmol g^{-1} (H_2 : CO = 2 : 1) in 16 h, 29.2-fold higher than that of its homogeneous counterpart. The H_2/CO ratios can be well controlled by carefully adjusting the molar ratio of PS/catalyst in the MOF platform and water content in the photocatalytic system. This work provides a prospective strategy for recycling CO_2 into H_2-rich syngas by merging PSs and single-site catalyst into the MOF platform.

2. Experimental section

2.1. Materials and methods

All chemicals were commercially available and used without further purification. Ru(bpy)$_2$Cl$_2$, Ru(H_2bpydc)(bpy)$_2$, UiO-67(bpydc) and Co-UiO-67(bpydc) were synthesized according to the references (bpy = 2,2′-bipyridine, H_2bpydc = 2,2′-bipyridine-5,5′-dicarboxylic acid) [43,44]. UV–vis diffuse reflectance spectra were taken using a UV–vis near-infrared spectrophotometer (Lambda 750 UV/VIS/NIR, Perkin Elmer, America). Powder X-ray diffraction (PXRD) data were collected by a Smart X-ray diffractometer (SmartLab 9 KW, Rigaku, Japan) with Cu Kα radiation (λ = 1.54178 Å). Energy dispersive X-ray spectroscopy (EDX) mapping images were acquired on an Environment Scanning Electron Microscope with a field emission gun (Quanta FEG 250, FEI, America). The photoluminescence (PL) spectra were conducted on a fluorescence spectrophotomer (F-7000, Hitachi, Japan). The time-resolved PL results were tested by time-resolved confocal fluorescence microscopy imager (Microtime 200, PicoQuant, Germany), the experimental data was analyzed by the SymPho time 64. N_2 adsorption-desorption isotherms were measured at 77 K using a liquid N_2 bath on a multi-station specific surface micropore and vapor adsorption analyzer (BELSORP-Max, MicrotracBEL, Japan). The Co and Ru content was determined by inductively coupled plasma mass spectrometer (ICP-MS, iCAP RQ, Germany). The amount of CO and H_2 generated in the photocatalytic process was quantified using Agilent 490 micro gas chromatograph (GC-2014, Shimadzu, Japan). Cyclic voltammograms (CVs) were recorded on a CHI 760E electrochemical workstation at room temperature.

2.2. Synthesis

Synthesis of Ru$_x$-UiO-67(bpydc). Different ratios x = 0.1, 0.2, 0.3 and 0.5 with a total amount of 0.13 mmol of Ru(H_2bpydc)(bpy)$_2$ and H_2bpydc (x = Ru(H_2bpydc)(bpy)$_2$/(Ru(H_2bpydc)(bpy)$_2$ + H_2bpydc) were added into a 6 mL of dimethylformamide (DMF) solution containing $ZrCl_4$ (30 mg, 0.13 mmol) and glacial acetic acid (0.3 mL, 5.2 mmol) in a 20 mL vial, which was heated at 100 °C for 24 h. After cooling down to room temperature, the resulting precipitate was collected by centrifugation and washed with DMF and methanol respectively before being dried under vacuum.

Synthesis of (Co/Ru)$_n$-UiO-67(bpydc). In a glove box, Co(NO_3)$_2$·6H_2O (29.1 mg, 0.10 mmol) was dissolved in 10 mL THF. Then, Ru$_x$-UiO-67(bpydc) (20.0 mg, x = 0.1, 0.2, 0.3 and 0.5) was added to the Co(NO_3)$_2$ solution. The resulting suspension was slowly stirred at room temperature overnight. The resulting solid was isolated by centrifugation and washed with THF for 5 times. The ratio of Co/Ru was determined to be 7.4, 5.8, 2.4, and 1.6, respectively by ICP-MS analysis (Table S1).

2.3. Photocatalytic reaction

Photocatalytic syngas production was performed in a 16 mL septum-sealed glass vial. In this typical process, 1 mg of (Co/Ru)$_n$-UiO-67(bpydc) was added into a 5 mL CH_3CN/H_2O (9/1, v/v) mixture with 0.3 M triethanolamine (TEOA) as the electron donor, the mixture was bubbled with CO_2 for 10 min and irradiated under a 450 nm LED lamp (100 mw/cm^2, 25 °C). The amount of CO and H_2 products was quantified by Agilent 490 micro gas chromatograph (5 Å molecular sieve column).

3. Results and discussion

3.1. Synthesis and characterization

A series of UiO-67(bpydc) MOFs functionalized with Ru-based PS and single site cobalt catalyst was achieved via a two-step self-assembly process to yield composite photocatalytic systems (Co/Ru)$_n$-UiO-67(bpydc) with controllable elemental ratio of Co/Ru. In these processes, the MOFs (Co/Ru)$_n$-UiO-67(bpydc) (n = 7.4, 5.8, 2.4 and 1.6) were design and synthesized by a mixed-ligand synthetic strategy and subsequently post-synthetic metalation (PSM). Firstly, the MOFs Ru$_x$-UiO-67(bpydc) (x = 0.1, 0.2, 0.3 and 0.5) with a specific composition were synthesized by carefully adjusting the ratio of H_2bpydc/Ru(H_2bpydc)(bpy)$_2$ to react with $ZrCl_4$ under solvothermal conditions (Fig. 1a). As the control experiments, UiO-67(bpydc) was also synthesized. The PSM of Ru$_x$-UiO-67(bpydc) and UiO-67(bpydc)

were performed by treating those nanocrystals with varied feed amounts of Co^{2+} solution in tetrahydrofuran (THF). The crystallinity of these UiO-67 MOFs maintained well in both Ru$_x$-UiO-67(bpydc) and (Co/Ru)$_n$-UiO-67(bpydc), which was confirmed by PXRD patterns similar to that of as-synthesized UiO-67 (Fig. 1b and S3). Successful incorporation of Ru and Co moieties were supported by diffuse reflectance UV/vis spectroscopy, elemental mapping, ICP-MS analysis and nitrogen sorption experiments. A broad absorption (~400-600 nm) in the spectrum of (Co/Ru)$_{2.4}$-UiO-67(bpydc) was consistent with the

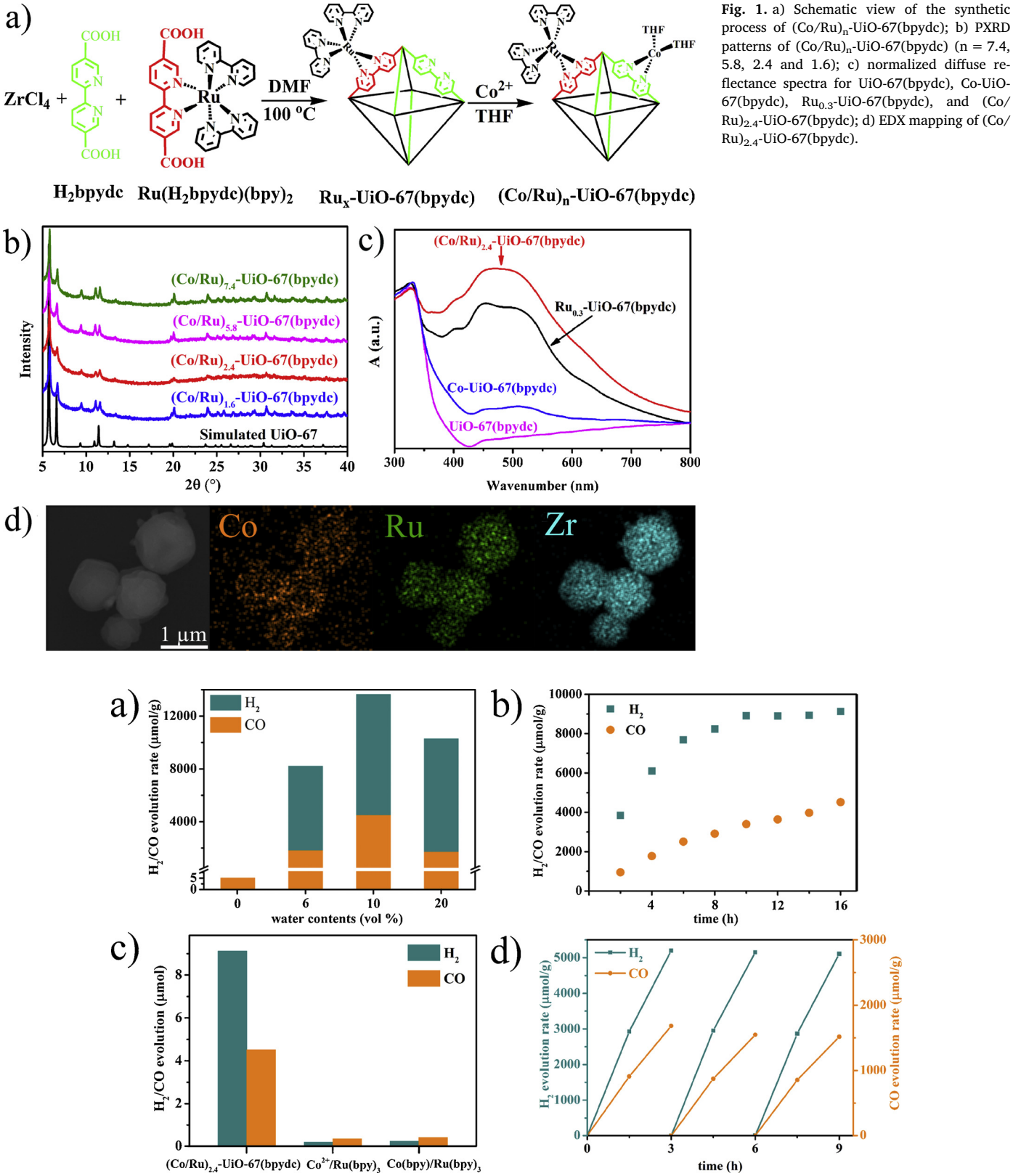

Fig. 1. a) Schematic view of the synthetic process of $(Co/Ru)_n$-UiO-67(bpydc); b) PXRD patterns of $(Co/Ru)_n$-UiO-67(bpydc) (n = 7.4, 5.8, 2.4 and 1.6); c) normalized diffuse reflectance spectra for UiO-67(bpydc), Co-UiO-67(bpydc), $Ru_{0.3}$-UiO-67(bpydc), and $(Co/Ru)_{2.4}$-UiO-67(bpydc); d) EDX mapping of $(Co/Ru)_{2.4}$-UiO-67(bpydc).

Fig. 2. a) Comparison of H_2/CO evolution rate with different water contents; b) Time profile of H_2 and CO evolution rate; c) H_2 and CO production in MOF and homogeneous catalytic system; d) recycle experiments for H_2 and CO production with MOF $(Co/Ru)_{2.4}$-UiO-67(bpydc) as catalyst.

combined absorption of $Ru_{0.3}$-UiO-67(bpydc) and Co-UiO-67(bpydc), which can be attributed to the absorption of Ru and Co moieties incorporated in the UiO-67 framework (Fig. 1c). As shown in Fig. 1d, S4 and S5, elemental mapping images suggest that Ru, Zr and Co elements were uniformly distributed in the MOFs. ICP-MS analysis of the digested $(Co/Ru)_n$-UiO-67(bpydc) reveals that the Co/Ru ratios in this MOF are 7.4, 5.8, 2.4 and 1.6, respectively.

Nitrogen sorption experiments were further performed on the

samples of UiO-67(bpydc), $Ru_{0.3}$-UiO-67(bpydc) and $(Co/Ru)_{2.4}$-UiO-67(bpydc), it could be obviously observed that both $Ru_{0.3}$-UiO-67(bpydc) and $(Co/Ru)_{2.4}$-UiO-67(bpydc) have much reduced BET surface areas (395.8 and 103.3 m^2/g, respectively) and obviously decreased pore sizes of 8.6 and 5.2 Å compared to that of UiO-67(bpydc) (2109.1 m^2/g, 14.5 Å) (Fig. 3a and S6). The reduction of in surface areas, pore volume and pore size of $Ru_{0.3}$-UiO-67(bpydc) and $(Co/Ru)_{2.4}$-UiO-67(bpydc) also demonstrates the presence of Ru/Co moieties in the MOFs. SEM images showed that the nanoparticle $(Co/Ru)_{2.4}$-UiO-67(bpydc) has a octahedral shape, in consistent with that of UiO-67 nanoparticles (Fig. S5).

3.2. Photocatalytic syngas production

As well known, $[Ru(bpy)_3]^{2+}$ complex has been widely used as PSs for capturing visible light and subsequently funneling excitation energy to catalytic active center to drive water splitting and CO_2RR. The Co-bpy compounds are usually used as high-efficiency catalysts for CO_2RR and HER in the presence of additional PSs. However, the long distance between PSs and catalysts in the homogeneous system seriously hinders the electron transfer efficiency between them, usually leading to extremely low photocatalytic performance. Here, the integration of PSs and catalytic active centers in a molecular platform was achieved, which can promote the electron transfer between antennas and catalytic active centers. The performance for tunable H_2/CO production over the PS and catalytic active center Co-functionalized MOF $(Co/Ru)_n$-UiO-67(bpydc) was evaluated in the CO_2 saturated mixed solvent of CH_3CN/H_2O under visible light irradiation. As shown in Fig. 2, H_2 and CO formed immediately under the visible light irradiation with a hybrid system of $(Co/Ru)_{2.4}$-UiO-67(bpydc) as catalyst. The HER activity achieves 9121.5 μmol H_2/g and CO_2RR activity reaches 4520.4 μmol CO/g with $(Co/Ru)_{2.4}$-UiO-67(bpydc) as the catalyst in the 9:1 CH_3CN/H_2O solution after a 16 h irradiation (Fig. 2b, Table 1). Photocatalytic studies reveal that the water contents in this catalytic system play an important role in the formation of H_2 and CO with a specific composition. However, this photocatalytic system can only produce little amount of CO in the absence of water (Table 1, Entry 1), which increased to a maximum of 4520.4 μmol/g with water content increasing to 10% (Table 1, Entry 3, Fig. 2a). As the same, photocatalytic activity for H_2 evolution also dramatically increased in the presence of 10% water (9121.5 μmol/g) to afford a specific composition of H_2 and CO with the ratio of ca. 2:1. The integration of PS and single site catalyst into a MOF platform greatly promote its activity for photocatalytic carbon CO_2 reduction into syngas, which was much higher than that of other catalyst@PS compostite in the MOF molecular platform (Table S2).

The ratio of Co/Ru in the MOF also importantly influence the composition of photocatalytic products of H_2/CO, which can be systematically adjusted from 3.0 to 1.9 with the Co/Ru ratio ranging from 7.4 to 1.6 (Table S3, Fig. S7a). The H_2/CO ratios can be further changed from 1.6 to 5.6 by enhancing the water content to 20% by changing the ratio of Co/Ru simultaneously (Table S4, Fig. S7b). We also explored the photocatalytic experiments with $[Ru(bpy)_3]^{2+}$ as the PS and Co^{2+}/Co(bpy) as catalysts in a homogeneous system, which can produce CO/H_2 of 0.35/0.20 μmol and 0.24/0.41 μmol for Co^{2+}- and Co(bpy)-containing systems, respectively (Fig. 2c). These results suggest that $(Co/Ru)_{2.4}$-UiO-67(bpydc) solid can significantly promote photochemical reactions for efficient syngas production with the gas evolution yield of 13,600 μmol g^{-1} (H_2 : CO = 2 : 1) in 16 h, 29.2- and 21-fold higher than that of its homogeneous counterparts of $Co^{2+}/[Ru(bpy)_3]^{2+}$ and $Co(bpy)/[Ru(bpy)_3]^{2+}$, respectively. Further, we conducted a series of control experiments and stability studies on the hybrid photocatalytic system. In this process, the control experiments were performed in the absence of catalyst $(Co/Ru)_{2.4}$-UiO-67(bpydc) (Table 1, Entry 5) or PS, using Ru-UiO-67(bpydc) without Co active center as catalyst, no TEOA or without irradiation, it could be found that no or trace amount of H_2 and CO can be detected from this photocatalytic system (Table 1). These results demonstrate that catalyst, PS and TEOA are all indispensable for syngas generation in this photocatalytic system. Further, when Ar was used instead of CO_2 with maintaining other conditions, only 1.4 μmol H_2 was produced, no CO could be detected in this reaction system (Table 1, Entry 6). Also, the isotopic labeling experiment was performed using high-purity $^{13}CO_2$, the evolution of CO was analyzed by gas chromatography and mass spectrometry. As shown in Fig. S8, the peak at m/Z = 29 could be assigned to generated ^{13}CO. All these results indicates that the CO produced in this photocatalytic process did come from CO_2 gas.

The stability and durability of $(Co/Ru)_{2.4}$-UiO-67(bpydc) were also

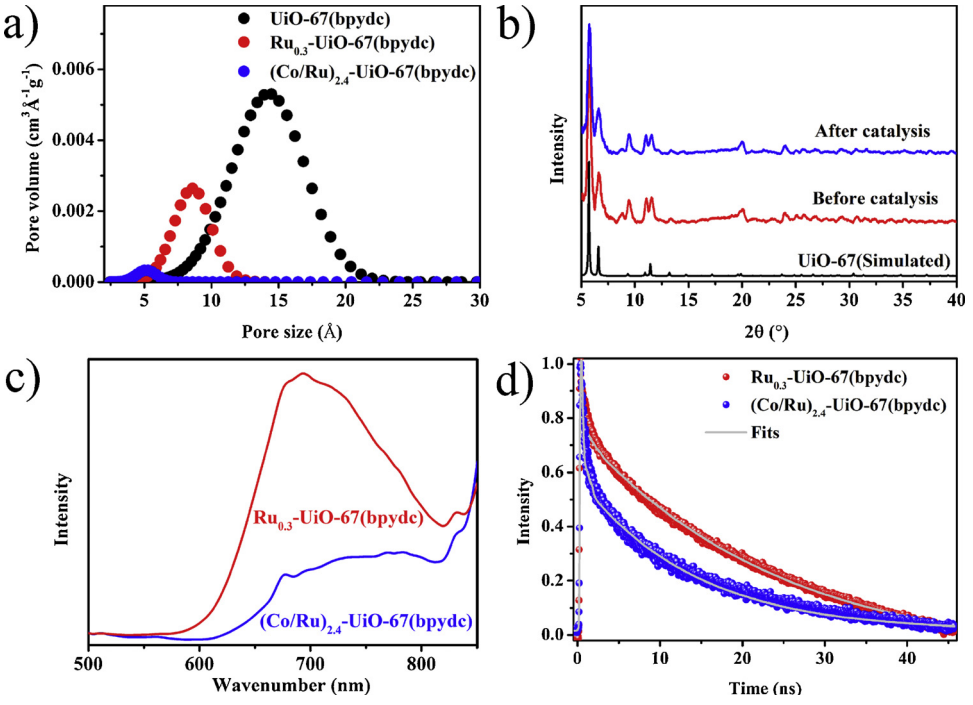

Fig. 3. a) Pore size distribution of UiO-67(bpydc) (black), $Ru_{0.3}$-UiO-67(bpydc) (red) and $(Co/Ru)_{2.4}$-UiO-67(bpydc) (blue); b) PXRD patterns of $(Co/Ru)_{2.4}$-UiO-67(bpydc) before and after the photocatalytic experiments; c) PL and time resolved PL spectra of $Ru_{0.3}$-UiO-67(bpydc) and $(Co/Ru)_{2.4}$-UiO-67(bpydc), with ET519LP as long wavelength pass filter, after excitation at 440 nm (For interpretation of the references to colour in this figure legend, the reader is referred to the web version of this article).

Table 1
The results of photocatalytic CO_2 reduction.

Entry	Catalyst	Water content (vol %)	H_2 (μmol/g)	CO (μmol/g)	$n(H_2)/n(CO)$
1	$(Co/Ru)_{2.4}$-UiO-67(bpydc)	0	0	5.1	0
2	$(Co/Ru)_{2.4}$-UiO-67(bpydc)	6	6345.0	1850.3	3.4
3	$(Co/Ru)_{2.4}$-UiO-67(bpydc)	10	9121.5	4520.4	2.0
4	$(Co/Ru)_{2.4}$-UiO-67(bpydc)	20	8536.5	1742.7	4.9
5	–	10	0	0	–
6	$(Co/Ru)_{2.4}$-UiO-67(bpydc)[a]	10	1377.0	0	–
7	Co-UiO-67(bpydc)	10	0	0	–
8	Ru-UiO-67(bpydc)	10	0	6.6	0
9	$(Co/Ru)_{2.4}$-UiO-67(bpydc)[b]	10	0	0	–
10	$(Co/Ru)_{2.4}$-UiO-67(bpydc)[c]	10	0	0	–

[a] Ar instead of CO_2.
[b] without light.
[c] without TEOA. Reaction conditions: 1 mg catalyst was added into 5 mL CO_2-saturated CH_3CN/H_2O mixed solvent containing 0.3 M TEOA at 25 °C, which was irradiated with a 450 nm LED light (100 $mWcm^{-2}$, irradiation area, 0.8 cm^2).

studied in the photocatalytic syngas production process. After each cycle, the photocatalyst was separated by centrifugation, and washed with acetonitrile for several times. Then, the regenerated $(Co/Ru)_{2.4}$-UiO-67(bpydc) was added to the same catalytic system. As shown in Fig. 2d, the catalytic activity of $(Co/Ru)_{2.4}$-UiO-67(bpydc) remained nearly unchanged after three cycles. Also, PXRD and SEM were performed on the $(Co/Ru)_{2.4}$-UiO-67(bpydc) before and after the photocatalytic experiments (Fig. 3b and S9). No obvious change of framework structure and the nanoparticle shape of $(Co/Ru)_{2.4}$-UiO-67(bpydc) could be observed after photocatalytic reaction. These results indicate that $(Co/Ru)_{2.4}$-UiO-67(bpydc) is stable during the photocatalytic reaction.

To further investigate the separation efficiency of photo-excited electron-hole pairs, PL spectra and time resolved PL were studied on the as-prepared MOFs. As shown in Fig. 3c, the $Ru_{0.3}$-UiO-67(bpydc) only containing the $[Ru(bpy)_3]^{2+}$ PS shows a strong phosphoresce peak centered at 700 nm upon excitation at 450 nm. Compared to that of $Ru_{0.3}$-UiO-67(bpydc), the PL spectrum of $(Co/Ru)_{2.4}$-UiO-67(bpydc) shows much weaker peak intensity, indicating an efficient phosphoresce quenching of $[Ru(bpy)_3]^{2+}$ center in the MOF by cobalt catalytic active center. Further, time-resolved PL confirms that Co complex can accelerate the PL decay of ^3MLCT exited state of $Ru(bpy)_3^{2+}$ with the lifetime from 25.4 ns to 13.1 ns (Fig. 3d, Table S5). Further, the PL and time-resolved PL of $(Co/Ru)_n$-UiO-67(bpydc) (n = 1.6 and 7.4) were also performed, which show similar patterns with that of $(Co/Ru)_{2.4}$-UiO-67(bpydc) (Fig. S10 and S11, Table S5). The time-resolved PL spectra of $(Co/Ru)_n$-UiO-67(bpydc) (n = 1.6 and 7.4) show much faster decay kinetics than Ru_x-UiO-67(bpydc) (x = 0.5 and 0.1). The corresponding quenching efficiency was calculated by integrating each PL spectra. As shown in Table S6, the quenching efficiency increases from 50.5% to 81.7% with the ratio of Co/Ru increasing from 1.6 to 7.4. These results presumably reveal the effective electron transfer from PS to catalyst to suppress the recombination of photo-excited charge carriers. To further illustrate photocatalytic mechanism, CV experiments were conducted on $(Co/Ru)_{2.4}$-UiO-67(bpydc). In the CV curve of $(Co/Ru)_{2.4}$-UiO-67(bpydc), there are three reduction peaks located at -1.43 V, -1.65 V and -1.87 V (vs SCE), which could be attributed to the reduction potentials of Ru-PS (Table S7). Also, a reduction peak corresponding to reduction of Co-bpydc in $(Co/Ru)_{2.4}$-UiO-67(bpydc) was also detected at the potential of -1.02 V vs SCE, which was similar to that $Co^{2+/1+}$ in Co-UiO-67(bpydc) (-0.98 V vs SCE). Based on these results, the oxidation potential of excited state Ru-PS was estimated to be -1.03 V, which is a little negative than that of Co-bpydc in both $(Co/Ru)_{2.4}$-UiO-67(bpydc) (E^{red} = -1.02 V) and Co-UiO-67(bpydc) (E^{red} = -0.98 V) [45]. Obviously, the driving force for electron transfer from Ru-PS to catalyst is very weak. However, integration of PS and catalyst into a molecular platform is beneficial to promote intramolecular electron transfer, resulting the efficient separation efficiency of photo-excited electron-hole pairs, which has been confirmed by phosphoresce quenching experiments. Thus, the photocatalytic performance of catalyst@PS composite was much enhanced compared to that of the homogeneous system, ca. 29.2- and 21-fold higher than that of Co^{2+}/$[Ru(bpy)_3]^{2+}$ and Co(bpy)/$[Ru(bpy)_3]^{2+}$, respectively.

Based on all above results, it could be found that the photogenerated electrons of Ru-PS could efficiently transferred to the cobalt catalyst as the integration of catalyst and PS into a molecular platform. As shown in Fig. 4, the cobalt-bpydc catalytic active center received electrons from PSs and subsequently donor them to both CO_2 molecules and protons absorbed on the surface of $(Co/Ru)_{2.4}$-UiO-67(bpydc) to reduce them into CO and H_2, respectively. In this process, TEOA as the electronic sacrificial agent can efficiently donor electrons to PSs to keep the reaction circulating.

4. Conclusions

In summary, we demonstrate a two-step self-assembly process to construct four photosensitizing MOFs to integrate PSs and single site catalyst with different proportions, featuring high visible-light photocatalytic activity for syngas production. Remarkably, the composition of syngas can be widely tuned by adjusting the water contents and Ru/Co ratios. The proportion of syngas with H_2 : CO = 2 : 1 was achieved by adjusting the Co/Ru ratio of 2.4 with water content of 10% in the

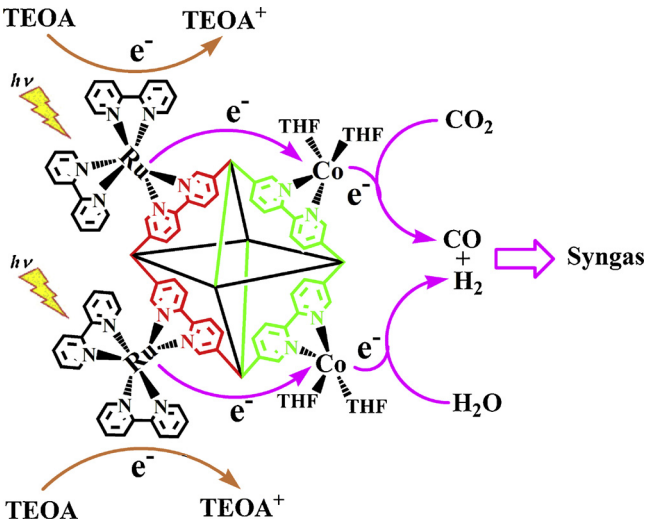

Fig. 4. Proposed mechanism for photocatalytic syngas production with $(Co/Ru)_n$-UiO-67(bpydc) as the catalyst under the visible light irradiation.

photocatalytic system, which accounts for the Fischer-Tropsch reaction. Under this condition, the efficient syngas production can reach an evolution yield of 13,600 μmol g^{-1} in 16 h, which is much higher compared to that of the homogeneous catalytic system. Further, a series of control experiments, PL and time-resolved PL investigations were performed to propose the reaction mechanism, indicating that the photogenerated electrons from the sensitizer can efficiently transfer to the Co-catalyst to reduce CO_2 and H_2O to syngas. This work successfully extends the application of PS and single-site catalyst co-functionalized MOFs to photocatalytic syngas production and provides a new perspective for developing more efficient MOF-based photocatalytic systems for CO_2RR and HER.

Acknowledgments

We are grateful for the financial support from National Key R&D Program of China (2017YFA0700104), National Natural Science Foundation of China (21722104 / 21671032 / 21331007 and 21790052), 111 project of China (No. D17003), Natural Science Foundation of Tianjin City of China (18JCJQJC47700 / 17JCQNJC05100), 131 Innovative Talent Project of Tianjin City of China.

Appendix A. Supplementary data

Supplementary material related to this article can be found, in the online version, at doi:https://doi.org/10.1016/j.apcatb.2019.01.014.

References

[1] J.R. Li, R.J. Kuppler, H.C. Zhou, Chem. Soc. Rev. 38 (2009) 1477–1504.
[2] Z.C. Kong, J.F. Liao, Y.J. Dong, Y.F. Xu, H.Y. Chen, D.B. Kuang, C.Y. Su, ACS Energy Lett. 3 (2018) 2656–2662.
[3] D. Zhao, S. Tan, D. Yuan, W. Lu, Y.H. Rezenom, H. Jiang, L.Q. Wang, H.C. Zhou, Adv. Mater. 23 (2011) 90–93.
[4] D.J. Levine, T. Runcevski, M.T. Kapelewski, B.K. Keitz, J. Oktawiec, D.A. Reed, J.A. Mason, H.Z. Jiang, K.A. Colwell, C.M. Legendre, S.A. FitzGerald, J.R. Long, J. Am. Chem. Soc. 138 (2016) 10143–10150.
[5] W.P. Lustig, S. Mukherjee, N.D. Rudd, A.V. Desai, J. Li, S.K. Ghosh, Chem. Soc. Rev. 46 (2017) 3242–3285.
[6] T. Zhang, W.B. Lin, Chem. Soc. Rev. 43 (2014) 5982–5993.
[7] J. Liu, L. Chen, H. Cui, J. Zhang, L. Zhang, C.Y. Su, Chem. Soc. Rev. 43 (2014) 6011–6061.
[8] M.T. Zhao, K. Yuan, Y. Wang, G.D. Li, J. Guo, L. Gu, W.P. Hu, H.J. Zhao, Z.Y. Tang, Nature 539 (2016) 76–80.
[9] H. Li, S. Yao, H.L. Wu, J.Y. Qu, Z.M. Zhang, T.B. Lu, W.B. Lin, E.B. Wang, Appl. Catal. B: Environ. 224 (2018) 46–52.
[10] H.B. Zhang, J. Wei, J.C. Dong, G.G. Liu, L. Shi, P.F. An, G.X. Zhao, J.T. Kong, X.J. Wang, X.G. Meng, J. Zhang, J.H. Ye, Angew. Chem. Int. Ed. 55 (2016) 14310–14314.
[11] R. Li, W. Zhang, K. Zhou, Adv. Mater. 30 (2018) 1705512.
[12] Y.Y. Zhu, G.X. Lan, Y.J. Fan, S.S. Veroneau, Y. Song, D. Micheroni, W. Lin, Angew. Chem. Int. Ed. 57 (2018) 14090–14094.
[13] M.C. Wen, K. Mori, Y. Kuwahara, H. Yamashita, ACS Energy Lett. 2 (2017) 1–7.
[14] M.C. Wen, K. Mori, Y. Kuwahara, T.C. An, H. Yamashita, Appl. Catal. B: Environ. 218 (2017) 555–569.
[15] Y.F. Chen, L.L. Tan, J.M. Liu, S. Qin, Z.Q. Xie, J.F. Huang, Y.W. Xu, L.M. Xiao, C.Y. Su, Appl. Catal. B: Environ. 206 (2017) 426–433.
[16] S.B. Wang, W.S. Yao, J.L. Lin, Z.X. Ding, X.C. Wang, Angew. Chem. Int. Ed. 53 (2014) 1034–1038.
[17] C.J. Chen, T.B. Wu, H.H. Wu, H.Z. Liu, Q.L. Qian, Z.M. Liu, G.Y. Yang, B.X. Han, Chem. Sci. (2018), https://doi.org/10.1039/C8SC02809E.
[18] X.L. Lv, K. Wang, B. Wang, J. Su, X. Zou, Y. Xie, J.R. Li, H.C. Zhou, J. Am. Chem. Soc. 139 (2016) 211–217.
[19] M.C. Wen, K. Mori, Y. Kuwahara, T.C. An, H. Yamashita, Chem. Asian J. 11 (2018) 2377–2381.
[20] C. Wang, K.E. deKrafft, W.B. Lin, J. Am. Chem. Soc. 134 (2012) 7211–7214.
[21] Z.M. Zhang, T. Zhang, C. Wang, Z.K. Lin, L.S. Long, W.B. Lin, J. Am. Chem. Soc. 137 (2015) 3197–3200.
[22] X.J. Kong, Z.K. Lin, Z.M. Zhang, T. Zhang, W.B. Lin, Angew. Chem. Int. Ed. 55 (2016) 6411–6416.
[23] D. Kim, D.R. Whang, S.Y. Park, J. Am. Chem. Soc. 138 (2016) 8698–8701.
[24] S.Z. Yang, B. Pattengale, S. Lee, J.E. Huang, ACS Energy Lett. 3 (2018) 532–539.
[25] S.Z. Yang, D.H. Fan, W.H. Hu, B. Pattengale, C.M. Liu, X.Y. Zhang, J.E. Huang, J. Phys. Chem. C 122 (2018) 3305–3311.
[26] J. Kim, T.A. Johnson, J.E. Miller, E.B. Stechel, C.T. Maravelias, Energy Environ. Sci. 5 (2012) 8417–8429.
[27] D. Kim, K.K. Sakimoto, D.C. Hong, P.D. Yang, Angew. Chem., Int. Ed. 54 (2015) 3259–3266.
[28] Y. Wang, N.Y. Huang, J.Q. Shen, P.Q. Liao, X.M. Chen, J.P. Zhang, J. Am. Chem. Soc. 140 (2018) 38–41.
[29] W. Zhu, C.F. Zhang, Q. Lia, L.K. Xiong, R.X. Chen, X.B. Wan, Z. Wang, W. Chen, Z. Deng, Y. Peng, Appl. Catal. B: Environ. 238 (2018) 339–345.
[30] S. Chu, S.Z. Fan, Y. Wang, D. Rossouw, Y. Wang, G.A. Botton, Z.T. Mi, Angew. Chem. Int. Ed. 55 (2016) 14262–14266.
[31] Y. Cao, Z.Y. Gao, J. Jin, H.C. Zhou, M. Cohron, H.Y. Zhao, H.Y. Liu, W.P. Pan, Energy Fuels 22 (2008) 1720–1730.
[32] P. Furler, J.R. Scheffe, A. Steinfeld, Energy Environ. Sci. 5 (2012) 6098–6103.
[33] G. Centi, S. Perathoner, Catal. Today 148 (2009) 191–205.
[34] A.M. Appel, J.E. Bercaw, A.B. Bocarsly, H. Dobbek, D.L. Dubois, M. Dupuis, J.G. Ferry, E. Fujita, R. Hille, P.J.A. Kenis, C.A. Kerfeld, R.H. Morris, C.H.F. Peden, A.R. Portis, S.W. Ragsdale, T.B. Rauchfuss, J.N.H. Reek, L.C. Seefeldt, R.K. Thauer, G.L. Waldrop, Chem. Rev. 113 (2013) 6621–6658.
[35] J.S. Lee, D.I. Won, W.J. Jung, H.J. Son, C. Pac, S.O. Kang, Angew. Chem. Int. Ed. 56 (2017) 976–980.
[36] M.E. Dry, Catal. Today 71 (2002) 227–241.
[37] T. Ouyang, H.H. Huang, J.W. Wang, D.C. Zhong, T.B. Lu, Angew. Chem., Int. Ed. 56 (2017) 738–743.
[38] U.J. Ryu, S.J. Kim, H.K. Lim, H. Kim, K.M. Choi, J.K. Kang, Sci. Rep. 7 (2017) 612.
[39] H.H. Fei, M.D. Sampson, Y. Lee, C.P. Kubiak, S.M. Cohen, Inorg. Chem. 54 (2015) 6821–6828.
[40] Z.H. Yan, M.H. Du, J. Liu, S. Jin, C. Wang, G.L. Zhuang, X.J. Kong, L.S. Long, L.S. Zheng, Nat. Commun. 9 (2018) 3353.
[41] H.Q. Xu, J.H. Hu, D.K. Wang, Z.H. Li, Q. Zhang, Y. Luo, S.H. Yu, H.L. Jiang, J. Am. Chem. Soc. 137 (2015) 13440–13443.
[42] Y. Su, Z. Zhang, H. Liu, Y. Wang, Appl. Catal. B: Environ. 200 (2017) 448–457.
[43] B.P. Sullivan, D.J. Salmon, T.J. Meyer, Inorg. Chem. 17 (1978) 3334–3341.
[44] P.H. Xie, Y.J. Hou, B.W. Zhang, Y. Cao, F. Wu, W.J. Tian, J.C. Shen, J. Chem. Soc. Dalton Trans. (1999) 4217–4221.
[45] R.S. Khnayzer, B.S. Olaiya, K.A.E.I. Roz, F.N. Castellano, ChemPlusChem 81 (2016) 1090–1097.